New physics from TOTEM's recent measurements of elastic and total cross sections

Preprint · August 2018

CITATIONS
0

READS
65

3 authors, including:

István Szanyi
Uzhhorod National University
26 PUBLICATIONS **133** CITATIONS

SEE PROFILE

New physics from TOTEM's recent measurements of elastic and total cross sections

Norbert Bence[a], László Jenkovszky[b], István Szanyi[a]

[a] *Uzhgorod National University, 14, Universytets'ka str., Uzhgorod, 88000, Ukraine*
[b] *Bogolyubov Institute for Theoretical Physics (BITP), Ukrainian National Academy of Sciences 14-b, Metrologicheskaya str., Kiev, 03680, Ukraine*

Abstract

We analyze the recently discovered phenomena in elastic proton-proton scattering at the LHC: the low-$|t|$ "break" (departure from the exponential behavior of the diffraction cone), the accelerating rise with energy of the forward slope $B(s)$, the absence of secondary dips and bumps on the cone and the role of the odderon in the forward phase of the amplitude, $\rho(13\ TeV) = 0.09 \pm 0.01$, especially its contribution at the dip region, measured recently by TOTEM. The dip at 13 TeV seems to become more shallow with respect to lower energies, and we attribute this important new phenomenon to the odderon contribution.

Keywords: LHC, TOTEM, pomeron, odderon, dip-bump, phase, slope
PACS: 13.75, 13.85.-t

1. Introduction

During the past seven years the TOTEM Collaboration produced a number of spectacular results on proton-proton elastic and total cross sections measured at the LHC in the range $2.76 \leq \sqrt{s} \leq 13$ TeV [1]. While the total, σ_{tot}, integrated elastic, σ_{el} and inelastic, σ_{in} cross sections, in general follow the expectations and extrapolations from lower energies, several new, unexpected features were discovered in elastic scattering. These are:

Email addresses: bencenorbert007@gmail.com (Norbert Bence), jenk@bitp.kiev.ua (László Jenkovszky), sz.istvan03@gmail.com (István Szanyi)

1. low-$|t|$ structure in $d\sigma/dt$ (the "break") [2, 3];

2. unexpectedly rapid rise of the forward slope $B(s,0))$ [1];

3. surprisingly low value of the phase of the forward amplitude [3].

4. absence of secondary dips/bumps in $d\sigma/dt$ [3, 4]; deepening or filling-in of the dip? (Following the first results at 13 TeV reported by TOTEM).

In this paper we analyse these and related phenomena within a Regge pole model, emphasizing their deviation from earlier trends and expectations, on the one hand and their discovery potential on the other hand.

The deviation of the diffraction cone from the exponential, colloquially called the "break" was first discovered in 1972 at the ISR [5]. It immediately attracted attention of theorists, who interpreted it as manifestation of the pionic atmosphere surrounding the nucleon [6, 7, 8, 9]. The effect was not seen for 40 years (e.g. at the Tevatron or SPS, although this might have been caused by poor statistics because the absence of Roman Pots there) but it reappeared at the LHC, with statistics exceeding that of the ISR experiment, enabling now its more detailed study, in particular its origin and universality.

The slope is defined as

$$B(s,t\to 0)=\frac{d}{dt}\left(\ln\frac{d\sigma}{dt}\right)\Big|_{t=0}, \tag{1}$$

where $A(s,t)$ is the elastic scattering amplitude. In the case of a single and simple Regge pole, the slope increases logarithmically with s:

$$B(s,t)=B_0(t)+2\alpha'(t)\ln(s/s_0). \tag{2}$$

The slope of the cone $B(s,t)$ is not measured directly, but it is deduced from the data on the directly measurable differential cross sections within certain bins in t. Therefore, the primary sources are the cross sections or the scattering amplitude fitted to these cross sections.

The slope $B(s,t)$ is extracted form the experimental data using finite bins in t [10], consequently it is function of both s and t.

For example, at the SPS Collider the slope was measured at $\sqrt{s} = 540$ GeV [11] in two t-bins with the result

$$B = 13.3 \pm 1.5 \text{ GeV}^{-2} \quad (0.15 < |t| < 0.26) \text{ GeV}^2,$$

$$B = 17.2 \pm 1.0 \text{ GeV}^{-2} \quad (0.05 < |t| < 0.18) \text{ GeV}^2.$$

Recall that at energies below the Tevatron, including those of SPS and definitely so at the ISR, secondary trajectories contribute significantly. At the LHC and beyond, we are at the fortunate situation where these non-leading contribution may be neglected. Apart from the pomeron, the odderon critical at the dip [12] may be present. Recall also that a single Regge pole produces a monotonic $\ln s$ rise of the slope, discarded by the recent LHC data [1].

The identification of the odderon is an important open problem for theory and phenomenology. In Ref. [13] a nearly model-independent method to extract the odderon from pp and $\bar{p}p$ data was suggested. The role of the odderon at the LHC is discussed in detail in the present paper.

We rely on the dipole pomeron (DP) as the optimal model producing the observed diffractive structure of the differential cross section (dip-bump).

A model-independent Levy expansion to describe the structure of the diffraction cone was suggested recently [15] providing a statistically acceptable description of the differential cross-section of pp and $\bar{p}p$ elastic scattering from ISR to LHC energies, but only with a fairly large number of Levy expansion coefficients. This description encodes the non-exponential behavior of the cone region to a single fit parameter, α, that was found to be less than unity, confirming the non-exponential behaviour not only at LHC but also at lower energies. Let us mention that for these values of α, the forward scattering amplitude is not an analytic function at $t = 0$, correspondingly the variance of the elastic amplitude in the impact parameter space is divergent, which is a common property of all Levy-stable source distributions. This yields a strongly t dependent nuclear slope $B(t)$ that tends to divergent values as $t \to 0$.

The appearance of a the diffraction structure (dips and bumps) may be indicative also of the internal structure of the nuclei. The details of this structure may reveal the proton's structure: number of constituents (quarks), their size etc. Such a program was put forward some time ago in Refs [16] and [17] and, recently M. Csanád *et al.* [18], who conclude that the observed dip-bump structure indicates the existence of diquarks inside the nucleons.

In the present paper we analyze elastic proton-proton scattering with special emphasis on the above issues, discovered by TOTEM and confirmed by ATLAS [19, 20].

In Sec. 2 we present the dipole pomeron model (DP) (for a review see *e.g.* [14]), main tool in our analysis, supplemented by preliminary fits to high-energy forward pp observables (elastic, inelastic and total cross sections), Sec. 3. The DP pomeron model is the unique alternative to a simple pole, since higher order poles are not allowed by unitarity. The DP produces (logarithmically) rising cross sections even at unit intercept. The DP scales reproducing itself with respect to s-channel unitarity corrections, for details see: Ref. [21] and the Appendix in Ref. [22]. A particularly attractive feature of the DP is the built-in mechanism of the diffraction pattern: a single minimum appears, followed by a maximum in the differential cross section, confirmed by the experimental data in a wide span of energies. In Sec.5 we scrutinize the recently reported measurement of the forward slope, apparently exceeding the standard logarithmic rise typical of Regge-pole models. In Sec. 4 we argue that the widely disputed value $\rho(13.0) = 0.1$ by itself cannot be considered of an odderon signal. Much more critical in this (odderon signal) respect is the dynamics of the dip and bump discussed in Sec. 7. Our analyses is completed by Sec.8, where we quantify our statement about the negligible role of secondary trajectories at the LHC and the progressively increasing contribution from the odderon.

2. The DP model and fits to the data

In our opinion, the Regge-pole model is the most adequate, although not unique way to analyze high-energy elastic hadron scattering. "Non-Regge" alternatives, with good fits to the data are e.g. the geometrical model of Chou and Young. In our opinion, Regge-pole models are attractive for being economic, especially in describing $C-$even and $C-$ odd (the odderon!) contributions with a single set of free parameters.

The construction of any scattering theory consists of two stages: one first chooses an input amplitude ("Born term"), subjected to a subsequent unitarization procedure. Neither the input, nor the unitarization procedure are unique. In any case, the better the input, i.e. closer to the true amplitude, the better are the chances of the unitarization. The standard procedure is that of Regge-eikonal, *i.e.* when the eikonal is identified with a simple Regge-pole input.

A possible alternative to the simple Regge-pole model as input is a double pole (double pomeron pole, or simply dipole pomeron, DP) in the angular momentum (j) plane. It has a number of advantages over the simple pomeron Regge pole. In particular, it produces logarithmically rising cross sections already at the "Born" level.

In this section we prepare the ground by introducing the model amplitude and fitting its parameters to the data. At the LHC, the pomeron dominates, however, to be consistent with the lower energy data, particularly those from the ISR, we include also two secondary reggeons. The odderon, the pomeron's odd-C counterpart is also included in the fitting procedure.

The scattering amplitude is [12]:

$$A\left(s,t\right)_{pp}^{\bar{p}p}=A_{P}\left(s,t\right)+A_{f}\left(s,t\right)\pm\left[A_{\omega}\left(s,t\right)+A_{O}\left(s,t\right)\right]. \tag{3}$$

Secondary reggeons are parametrized in a standard way [23, 24], with linear Regge trajectories and exponential residua. The f and ω reggeons are the

principal non-leading contributions to pp or $\bar{p}p$ scattering:

$$A_f\left(s,t\right)=a_f\mathrm{e}^{-i\pi\alpha_f(t)/2}\mathrm{e}^{b_f t}\Big(s/s_0\Big)^{\alpha_f(t)}, \tag{4}$$

$$A_\omega\left(s,t\right)=ia_\omega\mathrm{e}^{-i\pi\alpha_\omega(t)/2}\mathrm{e}^{b_\omega t}\Big(s/s_0\Big)^{\alpha_\omega(t)}, \tag{5}$$

with $\alpha_f\left(t\right)=0.703+0.84t$ and $\alpha_\omega\left(t\right)=0.435+0.93t$.

As already mentioned, the pomeron is a dipole in the $j-$plane

$$A_P(s,t)=\frac{d}{d\alpha_P}\Big[\mathrm{e}^{-i\pi\alpha_P/2}G(\alpha_P)\Big(s/s_{0P}\Big)^{\alpha_P}\Big]= \tag{6}$$
$$\mathrm{e}^{-i\pi\alpha_P(t)/2}\Big(s/s_{0P}\Big)^{\alpha_P(t)}\Big[G'(\alpha_P)+\Big(L_P-i\pi/2\Big)G(\alpha_P)\Big].$$

Since the first term in squared brackets determines the shape of the cone, one fixes

$$G'(\alpha_P)=-a_P\mathrm{e}^{b_P[\alpha_P-1]}, \tag{7}$$

where $G(\alpha_P)$ is recovered by integration. Consequently the pomeron amplitude Eq.(6) may be rewritten in the following "geometrical" form (for details see [14] and references therein):

$$A_P(s,t)=i\frac{a_P\ s}{b_P\ s_{0P}}[r_{1P}^2(s)\mathrm{e}^{r_{1P}^2(s)[\alpha_P-1]}-\varepsilon_P r_{2P}^2(s)\mathrm{e}^{r_{2P}^2(s)[\alpha_P-1]}], \tag{8}$$

where $r_{1P}^2(s)=b_P+L_P-i\pi/2$, $r_{2P}^2(s)=L_P-i\pi/2$, $L_P\equiv\ln(s/s_{0P})$ and the pomeron trajectory:

$$\alpha_P\equiv\alpha_P(t)=1+\delta_P+\alpha'_P t. \tag{9}$$

The odderon contribution is assumed to be of the same form as that of the pomeron apart from different values of adjustable parameters (labeled by the

subscript "O") and the negative charge parity:

$$A_O(s,t) = \frac{a_O\ s}{b_O\ s_{0O}}[r_{1O}^2(s)\mathrm{e}^{r_{1O}^2(s)[\alpha_O-1]} - \varepsilon_O r_{2O}^2(s)\mathrm{e}^{r_{2O}^2(s)[\alpha_O-1]}], \tag{10}$$

where $r_{1O}^2(s) = b_O + L_O - i\pi/2$, $r_{2O}^2(s) = L_O - i\pi/2$, $L_O \equiv \ln(s/s_{0O})$ and the trajectory

$$\alpha_O \equiv \alpha_O(t) = 1 + \delta_O + \alpha'_O t. \tag{11}$$

In earlier versions of the DP, to avoid conflict with the Froissart bound, the intercept of the pomeron was fixed at $\alpha(0) = 1$. However later it was realized that the logarithmic rise of the total cross sections provided by the DP may not be sufficient to meet the data, therefore a supercritical intercept was allowed for. From the fits to the data the value $\delta = \alpha(0) - 1 \approx 0.04$, half of Landshoff's value [25] follows. This is understandable: the DP promotes half of the rising dynamics, thus moderating the departure from unitarity at the "Born" level (smaller unitarity corrections).

We use the norm where

$$\frac{d\sigma_{el}}{dt}(s,t) = \frac{\pi}{s^2}|A(s,t)|^2 \ \text{ and } \ \sigma_{tot}(s) = \frac{4\pi}{s}\Im mA(s,t=0)\ . \tag{12}$$

The parameter $\rho(s)$, the ratio of the real and imaginary part of the forward scattering amplitude is

$$\rho(s) = \frac{ReA(s,t=0)}{ImA(s,t=0)}. \tag{13}$$

The free parameters of the model defined by the formulas Eqs. (3-13) were fitted simultaneously to the following dataset:

- TOTEM 7 TeV elastic pp differential cross section data [4] in the region of $0.35 \leqslant |t| \leqslant 2.5$ GeV^2;
- SPS 546 and 630 GeV elastic $p\bar{p}$ differential cross section data [26] in the region of $0.5 \leqslant |t| \leqslant 2.2$ GeV^2;
- pp and $p\bar{p}$ total cross section and ρ parameter data [1, 3, 4, 27, 28, 29, 30,

31] in the region of $20 \leqslant \sqrt{s} \leqslant 57000$ GeV.

The fit was done with MINUIT2 and MIGRAD algorithm. To optimize our fit the above intervals in t were chosen and 63 outlier differential cross section data point were also reduced. In the LHC energy region concerning the total cross section data apart from the cosmic ray measurements only the TOTEM measurements were used during the fit. The values of fitted parameters and the fit statistic are shown in Table 1.

Table 1: Fitted parameters to pp and $p\bar{p}$ data on elastic differential cross section, total cross section and the parameter ρ.

Pomeron		Odderon	
a_P	360 (fixed)	a_O	1.746 ± 0.1052
b_P	4.122 ± 0.147	b_O	0.9818 ± 0.01221
δ_P	0.02902 ± 0.0005633	δ_O	0.2739 ± 0.004785
α'_P	0.5082 ± 0.002791	α'_O	0.2303 ± 0.001822
ε_P	0.2843 ± 0.01498	ε_O	1.343 ± 0.001593
s_{0P}	100 (fixed)	s_{0O}	100 (fixed)
Reggeons		**Fit statistics**	
a_f	-20.1 ± 0.17		
b_f	20 (fixed)	χ^2	223.2
a_ω	10.64 ± 0.638	NDF	159
b_ω	10 (fixed)	χ^2/NDF	1.4
s_0	1 (fixed)		

3. Elastic, inelastic and total cross sections

Fig. 1 shows the results of our fits to pp and $p\bar{p}$ total cross section data [1, 27, 28, 29, 31].

Elastic cross section $\sigma_{el}(s)$ is calculated by integration

$$\sigma_{el}(s) = \int_{t_{min}}^{t_{max}} \frac{d\sigma}{dt}(s,t)\, dt, \tag{14}$$

whereupon

$$\sigma_{in}(s) = \sigma_{tot}(s) - \sigma_{el}(s). \tag{15}$$

Formally, $t_{min} = -s/2$ and $t_{max} = t_{threshold}$, however since the integral is saturated basically by the first cone, we set $t_{max} = 0$ and $t_{min} = -1$ GeV^2. The results are shown in Fig. 2.

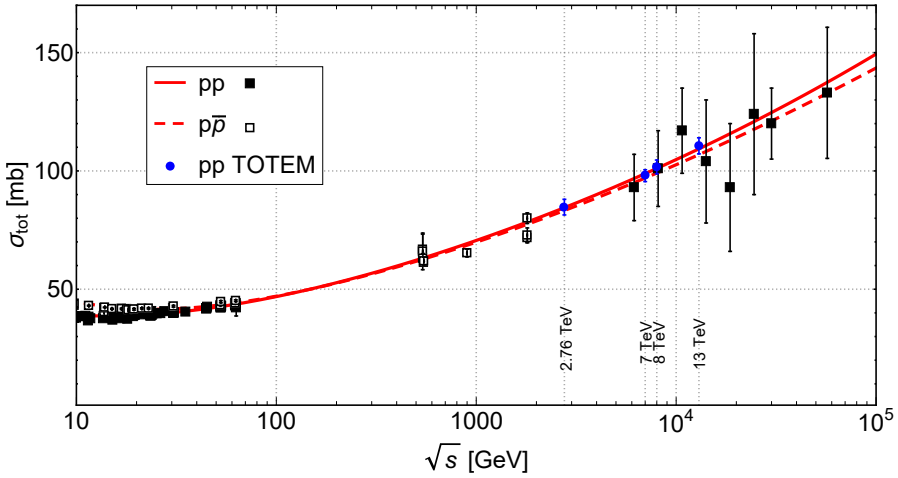

Figure 1: Fits to pp and $p\bar{p}$ total cross section data [1, 27, 28, 29, 31] using the model Eqs. (3-13).

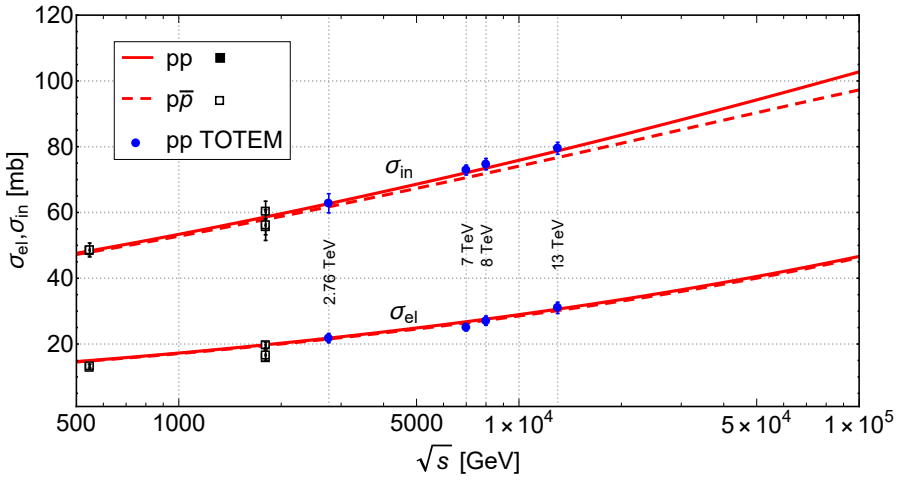

Figure 2: Calculated elastic and inelastic pp and $p\bar{p}$ cross sections using Eqs. (14-15) compared to the data [1, 27, 28, 29].

4. The phase $\rho(13\ TeV, t = 0)$

The widely discussed recent measurement of the phase $\rho(13\ TeV) = 0.09 \pm 0.01$ (or $\rho(13\ TeV) = 0.1 \pm 0.01$) [3]. This data point lies well below the expectations (extrapolations) from lower energies, although this should not be dramatized. The flexibility of the odderon parametrization leaves room for perfect fits to this data point simultaneously fitting the total cross section as (see below). More critical the inclusion of non-forward data, both for pp and $\bar{p}p$ especially around the dip region, to which the odderon is sensitive! Independent of theoretical interpretation, another, independent measurement of the phase is highly desirable.

Fig. 3 shows the results of our fits to pp and $p\bar{p}$ ρ-parameter data [3, 4, 28, 30]. Our model simultaneously can describe the new TOTEM measurement on the total cross section and the parameter-ρ, however only a few model does [3]. In Ref. [32] we managed to achieve similar good results by using simple pomeron and odderon poles. As we can see in Fig. 3 the case without the odderon (presented with the dotted line) does not give a description for the new 13 TeV data point. However the neglection of the oddereon has no significant effect for the description of the new TOTEM total cross section measurements.

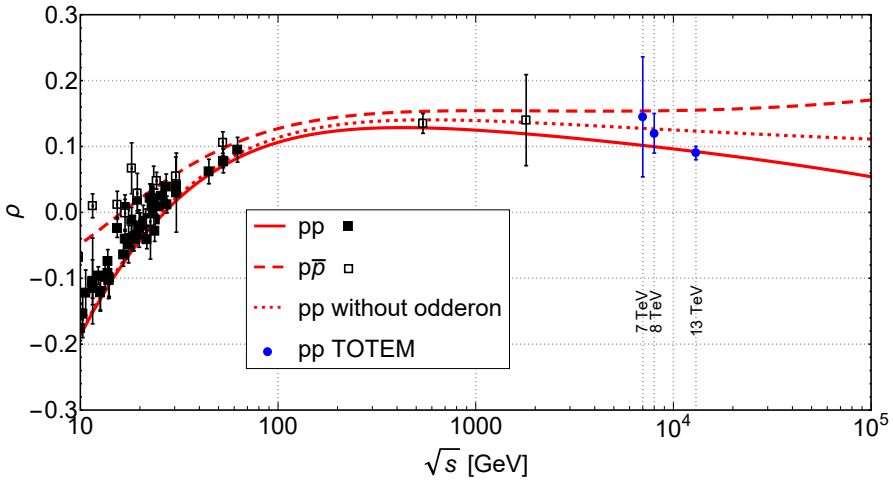

Figure 3: Fits to pp and $p\bar{p}$ ratio ρ data [3, 4, 28, 30] using the model Eqs. (3-11) and Eq. (13).

We calculated also the t-dependence of the ρ-parameter and the hadronic phase defined as $\phi(s,t) = \pi/2 - \arg A(s,t)$ at several energies for pp and $\bar{p}p$ scattering shown in Fig. 4 and Fig. 5. The hadronic phase may be important in studies of the impact parameter amplitude [33].

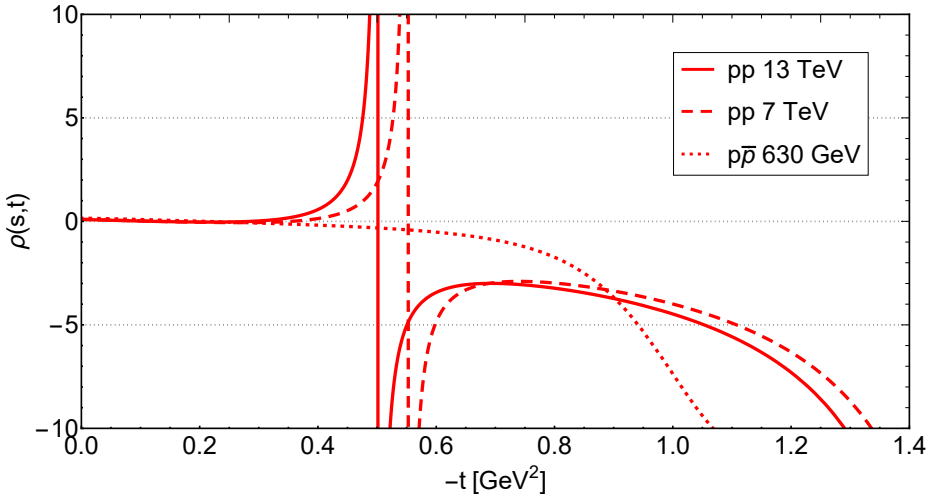

Figure 4: The t-dependent ρ-parameter at several energies calculated with the model Eqs. (3-11) and Eq. (13) (when $t \neq 0$).

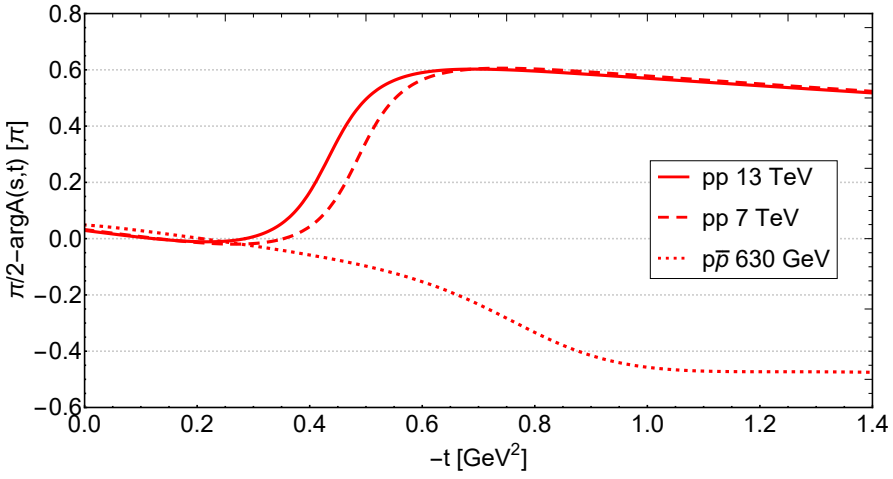

Figure 5: The t-dependent hadronic phase at several energies calculated with the model Eqs. (3-11).

The above calculations are intended to provide the ground for our study of the slope, to be presented in the next Section.

5. The slope $B(s)$

While in Regge-pole models the rise of the total cross sections is regulated by the hardness of the Regge pole (here, the pomeron), the slope $B(s)$ in case of a single and simple Regge pole is always logarithmic. Deviation (acceleration) may arise from more complicated Regge singularities, the odderon and/or from unitarity corrections.

With the model and its fitted parameters in hand, we calculated the pp and $p\bar{p}$ elastic slope $B(s)$ using Eq. 1. Result is shown in Fig. 6. More detail from the slope given by Eq. (1) with the norm Eq. (12) and the amplitude Eq. (3) can be find in the Appendix.

By using the parametrization

$$B(s) = b_0 + b_1 \ln(s/s_0) + b_2 \ln^2(s/s_0) \tag{16}$$

we did a fit to the pp and $p\bar{p}$ elastic slope data in the energy region of $546 \leqslant \sqrt{s} \leqslant 13000$ GeV. Neglecting the lower, outlier 546 GeV data points the fitted values of parameters $b_0 = 13.75$, $b_1 = -0.358$, $b_2 = 0.0379$ and $\chi^2/NDF = 1.97$. Its result is also shown in Fig. 6.

To see better the effect of the odderon, the deviation of $B(s)$ from its "canonical", logarithmic form, we show in Fig. 7 its "normalized" shape, $B(s)/(a \ln(s/s_0))$ setting $a = 1$ GeV^{-2} and $s_0 = 1$ GeV^2. A similar approach was useful in studies [2, 32, 34, 35] of the fine structure (in t) of the diffraction cone.

In Fig.7 pp curve stars to increase from $\sqrt{s} \approx 50$ TeV which indicates that the slope stars to rise as $\ln^2 s$. Only the dipole pomeron without the odderon (dotted curve in Fig. 7) at the "Born" level, fitting data on elastic, inelastic and total cross section, does not reproduce the irregular behavior of the forward slope observed at the LHC. Remarkably, the inclusion of the odderon produces a $\ln^2 s$ behavior of the elastic slope $B(s)$ beyond the LHC energy region.

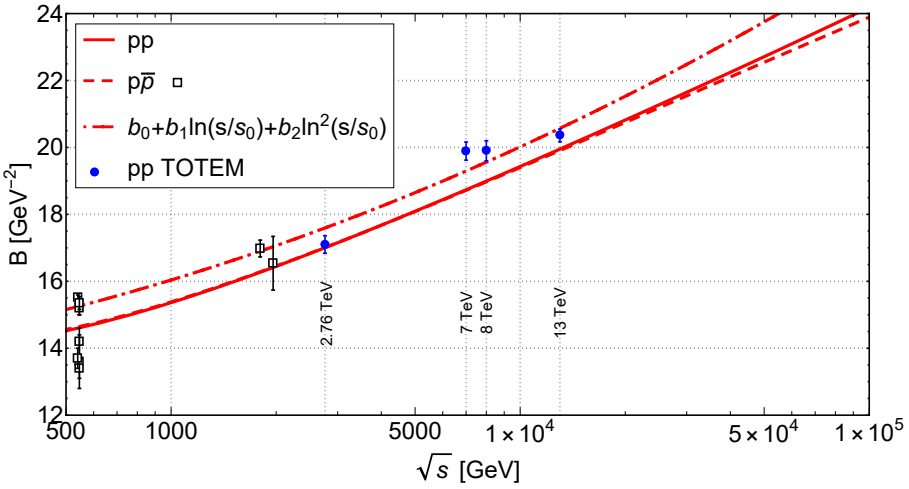

Figure 6: pp and $p\bar{p}$ elastic slope $B(s)$ a) calculated from the fitted model Eqs. (3-12) using Eq. (1) and b) fitted with the parametrization Eq. (16).

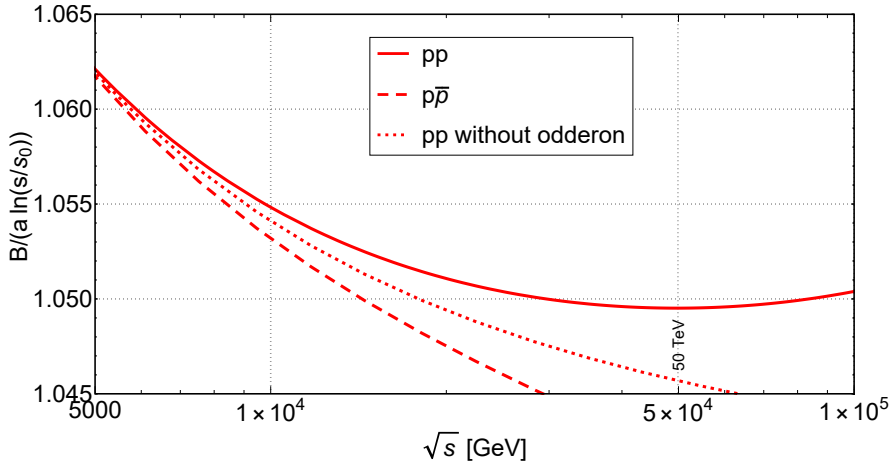

Figure 7: The ratio $B(s)/(a\ln(s/s_0))$ calculated from the fitted model Eqs. (3-12) using Eq. (1).

6. The "break"

The deviation from the linear exponential behavior was confirmed by recent measurements by the TOTEM Collaboration at the CERN LHC, first at 8 TeV

(with a significance greater than 7σ) [2] and subsequently at 13 TeV [3].

At the ISR the "break" was illustrated by plotting the local slope [5]

$$B(t) = \frac{d}{dt} \ln(d\sigma/dt) \tag{17}$$

for several t-bins at fixed values of s. At the LHC, the effect is of the same order of magnitude and is located near the same value of $-t \approx 0.1$ GeV^2. Different from the ISR the TOTEM quantifies the deviation from the exponential by normalizing the measured cross section to a linear exponential form [2, 3].

The normalized form as used by TOTEM:

$$R(t) = \frac{d\sigma/dt}{d\sigma/dt_{ref}} - 1, \tag{18}$$

where $d\sigma/dt_{ref} = Ae^{Bt}$, with A and B are constants determined from a fit to the experimental data.

The observed "break" can be identified [6, 8, 9, 32, 34, 35] with the two-pion exchange in the t-channel. As shown by Barut and Zwanziger [36], t-channel unitarity constrains the Regge trajectories near the threshold, $t \to t_0$ by

$$Im\, \alpha(t) \sim (t - t_0)^{\Re e\, \alpha(t_0)+1/2}, \tag{19}$$

where t_0 is the lightest threshold, $4m_\pi^2$ in the case of the vacuum quantum numbers (pomeron or f meson). Since the asymptotic behavior of the trajectories is constrained by dual models with Mandelstam analyticity by square-root (modulus $\ln t$): $\mid \frac{\alpha(t)}{\sqrt{t}\ln t} \mid_{t\to\infty} \leq$ const, (see Ref. [6] and references therein), for practical reasons it is convenient to approximate, for the region of t in question, the trajectory as a sum of square roots. Higher thresholds, indispensable in the trajectory, may be approximated by their power expansion, *i.e.* by a linear term, matching the threshold behavior with the asymptotic.

By using a simple Regge-pole model with two leading (pomeron and odderon) and two secondary reggeons, f and ω exchanges we have mapped the "break"

fitted at the ISR onto the LHC TOTEM 8 and 13 TeV data. The model, the detailed results of fits and the parameters are presented in Ref [32]. In normalized form, Fig. 8 and Fig. 9 show our description to the "break" measured at 8 and 13 TeV. These results re-confirm the earlier finding that the "break" can be attributed the presence of two-pion branch cuts in the Regge parametrization.

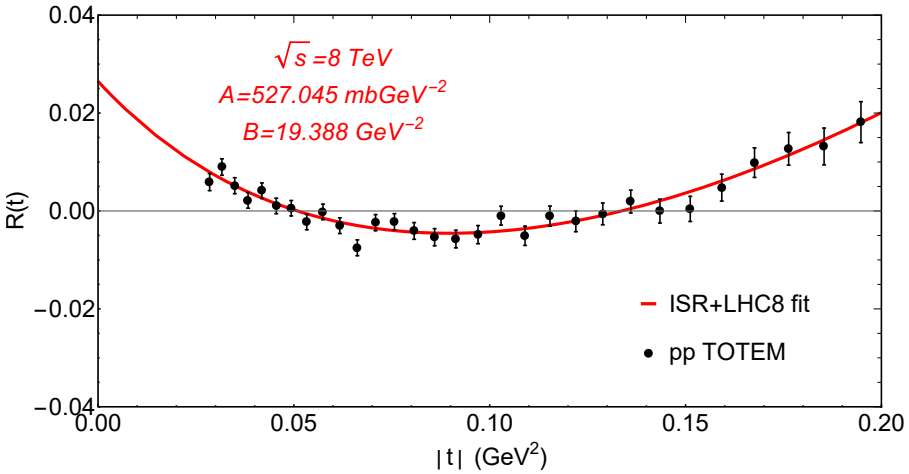

Figure 8: Normalized differential cross section $R(t)$ calculated from low-$|t|$ 8 TeV TOTEM data [2] using Eq. (18). This figure is from Ref. [32].

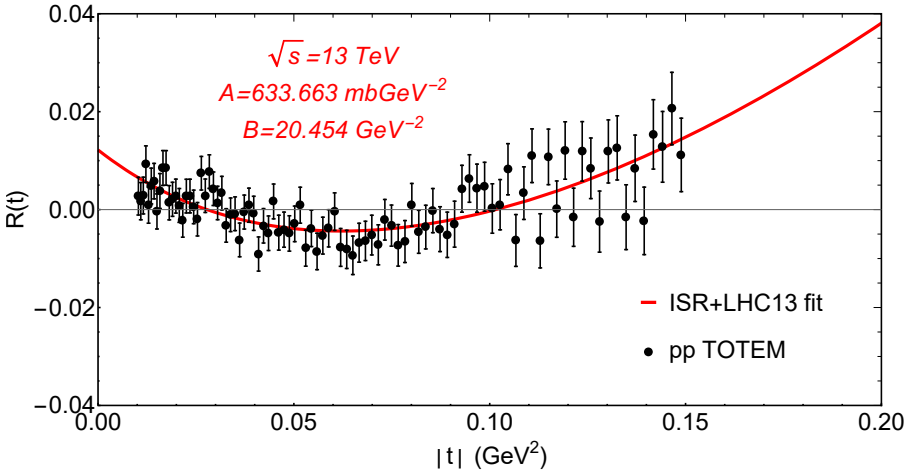

Figure 9: Normalized differential cross section $R(t)$ calculated from low-$|t|$ 13 TeV TOTEM data [3] using Eq. (18). This figure is from Ref. [32].

In Ref [32] two further aspects of the phenomenon were investigated, namely: 1) to what extent is the "break" observed recently at the LHC a "recurrence" of that seen at the ISR (universality)? 2) what is the relative weight of the Regge residue (vertex) compared to the trajectory (propagator) in producing the "break"? We showed that the deviation from a linear exponential of the pp diffraction cone as seen at the ISR and at the LHC are of similar nature: they appear nearly at the same value of $t \approx -0.1$ GeV^2, have the same shape of comparable size, and may be fitted by similar t-dependent function. Furthermore we find that the Regge residue and the pomeron trajectory have nearly the same weight and importance.

7. The diffraction minimum and maximum (dip-bump)

The most sensitive (crucial) test for any model of elastic scattering is the well-known dip-bump structure in the differential cross section. It was measured in a wide range of energies and squared momenta transfers. None of the existing models was able to predict the position and dynamics of the dip for (especially when both pp and $\bar{p}p$ data are included). The first LHC measurements (at 7 TeV) [4] clearly demonstrated their failure. Recently TOTEM made public [3] new, preliminary data on elastic differential cross section at highest LHC energy 13 TeV extending up to $t = -3.5$ GeV^2. The main message from these data is that the second cone is smooth, structureless. This finding calls for the revision of models in which the dip is created by unitarization resulting in interference between single and multiple scattering or, alternatively by eikonal corrections, generating multiple diffraction minima and maxima.

Before going into details, let us remind that the present DP model predicts $d\sigma/dt|_{min.} \sim 1/L$, $d\sigma/dt|_{max.} \sim L$ and consequently $\frac{d\sigma/dt|_{max.}}{d\sigma/dt|_{min.}} \sim L^2$, where $L = \ln s$, in the case of a single pomeron contribution. The addition of the odderon, due to its opposite C parity, destroys the dip in case of $\bar{p}p$ scattering (degrading to a "shoulder" at the dip position). In pp the odderon contributes as given by Eq. (3), however the overall effect depends on the details or the

parametrization. We have performed a fit of the differential cross section in the dip region including both the pomeron and odderon. The result for pp and $p\bar{p}$ differential cross sections, using Eqs. (3)-(12) is shown in Fig. 10.

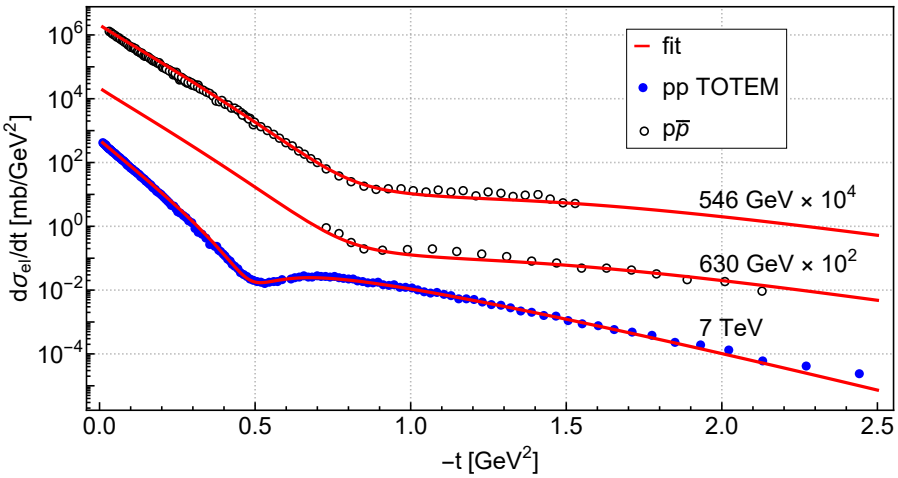

Figure 10: Results of the fit for pp and $p\bar{p}$ differential cross section data [4, 26] using the model Eqs. (3-12).

Next we study the energy dependence of the minimum and maximum of pp diffraction cone *i.e.* the behavior of $(d\sigma_{el}/dt)_{min}(s)$, $(d\sigma_{el}/dt)_{max}(s)$ and their ratio $(d\sigma_{el}/dt)_{max}(s)/(d\sigma_{el}/dt)_{min}(s)$. The mentioned quantities were calculated numerically from the fitted model and they are plotted in Fig. 11 and Fig. 12. As it will be shown in Sec. 8, in the dip-bump region at high energies ($\sqrt{s} \gtrsim 500$ GeV) the secondary reggeons can be fully neglected and thus here we investigate only the contributions of the pomeron and the odderon in the evolution of the minimum and maximum.

Fig. 12 shows that in the ratio $(d\sigma_{el}/dt)_{max}(s)/(d\sigma_{el}/dt)_{min}(s)$ the pomeron and the odderon components separately monotonically increase which means that both produce monotonically deepening minimum with increasing energy. However, the ratio $(d\sigma_{el}/dt)_{max}(s)/(d\sigma_{el}/dt)_{min}(s)$ monotonically decreases in the case when both the pomeron and the odderon components are present. To summarize, our conclusion about the dynamics of the dip-bump structure at

LHC energies is inconclusive. Further studies, both theoretical and experimental of this important and delicate phenomenon are necessary.

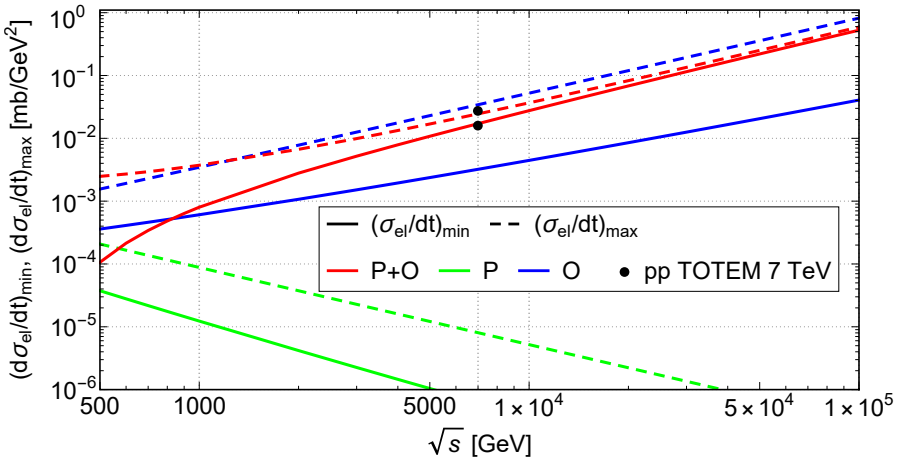

Figure 11: Energy dependence of the maximum and minimum of the pp diffraction cone calculated from the fitted model.

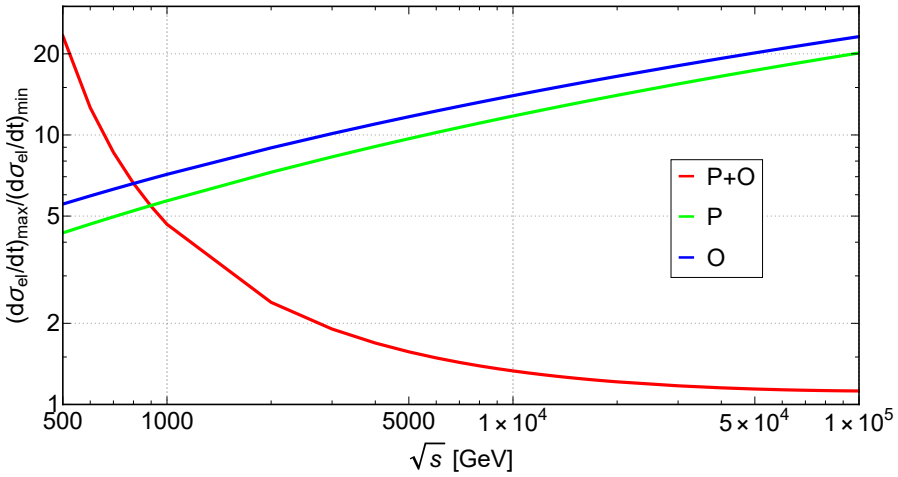

Figure 12: Energy dependence of the ratio of the maximum and minimum of the pp diffraction cone calculated from the fitted model.

8. Relative contribution from different components of the amplitude

Within the framework of the model Eqs. (3-11), we first calculated the relative contribution from the different components of the amplitude

$$R_i(s) = \frac{ImA_i(s, t = 0)}{ImA(s, t = 0)}, \tag{20}$$

to the pp and $p\bar{p}$ total cross-sections, where $i = f + \omega$ for the relative weight of the reggeons, $i = P$ for the relative weight of the pomeron and $i = O$ for the relative weight of the odderon. The result is shown in Fig. 13.

One can see from Fig. 13 that at "low" energies (typically 10 GeV) the contribution from reggeons and the pomeron are nearly equal, but as the energy increases the pomeron takes over and at the same time the importance of the odderon is slightly growing.

Such a discrimination (between the different contributions of the components of the amplitude) is more problematic in the non-forward direction, where the real and imaginary parts of various components of the scattering amplitude behave in a different way and the phase can not be controlled experimentally.

We calculate the relative contributions of different components of the amplitude for non-forward scattering ($t \neq 0$):

$$R_i(s, t) = \frac{\left|A_i(s, t)\right|^2}{\left|A(s, t)\right|^2}. \tag{21}$$

The relative contribution from secondary reggeons $R_{f+\omega}(s, t)$ versus $-t$ at 546 GeV, 7, 8 and 13 TeV is shown in Fig. 14. One can see that the role of the secondary reggeons rapidly decreases with increasing $|t|$ values.

Furthermore, we calculated the relative importance in t of the pomeron R_P and of the odderon R_O at 7 TeV. The result is shown in Fig. 15. One can see that at low $|t|$ values the pomeron completely dominates, then around the dip-bump region the pomeron-odderon importance is about 50-50% and finally at higher $|t|$ values the odderon takes over.

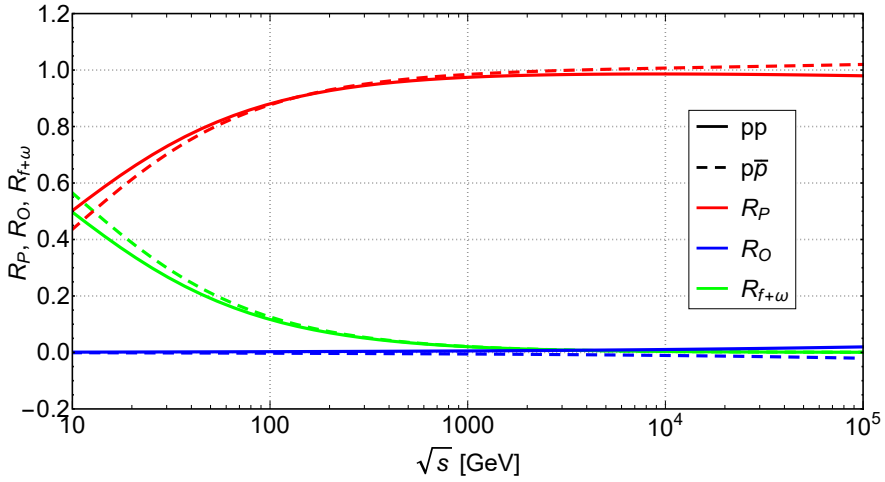

Figure 13: Relative contribution from different components of the amplitude to pp and $p\bar{p}$ total cross-sections calculated from the model, Eqs. (3-11), Eq. (20).

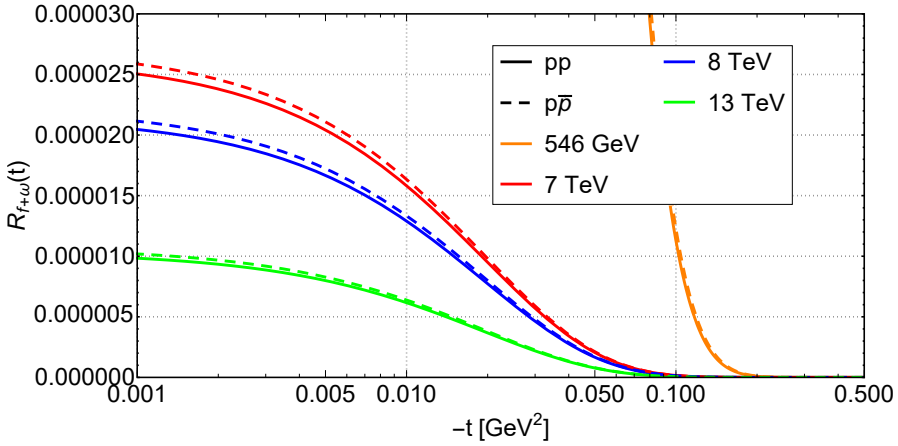

Figure 14: Relative contribution from secondary reggeons to the pp and $p\bar{p}$ differential cross-sections calculated from the model, Eqs. (3-11), Eq. (21).

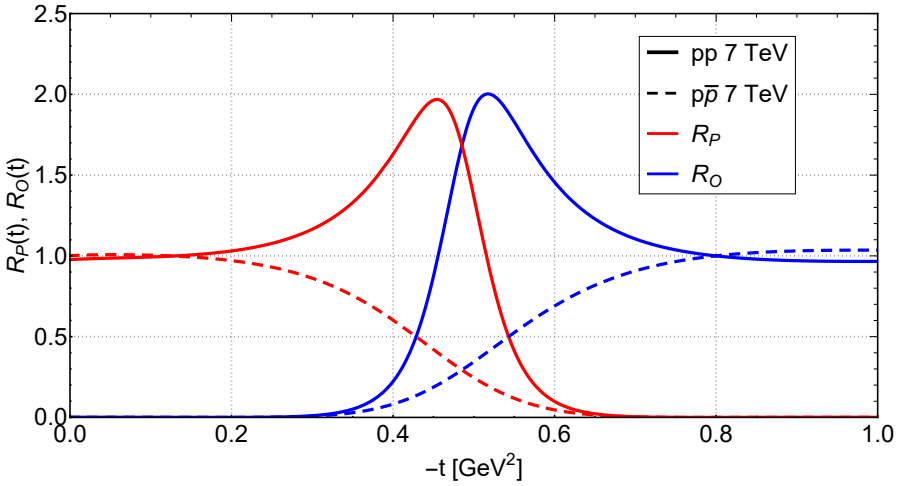

Figure 15: Relative contribution from the pomeron and from the odderon to the pp and $p\bar{p}$ differential cross-sections at 7 TeV calculated from the model, Eqs. (3-11), Eq. (21).

Conclusions

We conclude that:

1. The "break" is a universal feature of the forward cone. Regge-pole models interpolate this effect from the ISR energies up to those of the LHC. The "break" is due to the non-linear behavior of the pomeron trajectory and the non-exponential Regge residue, both resulting from a threshold singularity in the amplitude due to $t-$channel unitarity.

2. A single diffraction minimum (and maximum) in $d\sigma/dt$ is produced by a particular interference between a single and double pomeron poles. Unitarization, for example eikonalizaiton produces multiple dips and bumps. We did no include two rightmost data points ($-t > 2.25$ GeV^2) lying above the exponential curve; probably, they indicate the transition from "soft" to "hard" scattering, that in our model is mimicked by the transition from the linear to logarithmic regime of the Regge (here, pomeron) trajectory (see e.g. [12] and earlier references therein).

3. The observed non-monotonic rise of the slope $B(s,t)$ at the LHC is incompatible with a single pomeron pole. Even the combination of a simple

and double pole (DP) cannot accommodate for the accelerated rise of $B(s)$ at the LHC. The $\ln^2 s$ increase of the forward slope $B(s)$, reported by TOTEM, however may be reproduced by the odderon contribution to the scattering amplitude. The odderon may play and important role in the behavior of $B(s)$ at high energies, as shown in Fig. 7.

4. The recently reported low $\rho(13) = 0.1$ data point was not predicted but it was adjusted, (together with the total cross section data) in several papers published after the appearance of the experimental data, thus they should be considered as "proofs" of the odderon, whose existence was never questioned. Critical will be fits including the dip-bump region, especially for various energies and both for pp and $\bar{p}p$ scattering. In any case, confirmation of this the value $\rho(13) = 0.1$ by an independent experiment is welcome.

An even more important consequence for the dynamics, than any particular parametrization of the odderon, is that it may indicate (anticipate) the future slow-down (due to saturation effects) of the rise of cross sections with energy.

Acknowledgments

We thank Tamás Csörgő and Frigyes Nemes for useful discussions and correspondence. L. J. was supported by the Ukrainian Academy of Sciences' program "Structure and dynamics of statistical and quantum systems". The work of N. Bence and I. Szanyi was supported by the "Márton Áron Szakkollégium" program.

Appendix

The slope $B(s)$, calculated from Eq. (1) with the norm Eq. (12) and the amplitude Eq. (3) takes the form:

$$B(s) = \frac{a(s) + b(s)L + c(s)L^2 + d(s)L^3}{e(s) + f(s)L + g(s)L^2}, \tag{22}$$

where

$$
\begin{aligned}
a(s) &= \sum_{i=1}^{10} a_i s^{k_i}, \quad b(s) = \sum_{i=1}^{10} b_i s^{k_i}, \\
c(s) &= \sum_{i=4}^{10} c_i s^{k_i}, \quad d(s) = \sum_{i=8}^{10} d_i s^{k_i}, \\
e(s) &= \sum_{i=1}^{10} e_i s^{k_i}, \quad f(s) = \sum_{i=4}^{10} f_i s^{k_i}, \\
g(s) &= \sum_{i=8}^{10} g_i s^{k_i}.
\end{aligned} \tag{23}
$$

The parameters a_i, b_i, c_i, d_i, e_i, f_i, g_i, and k_i are related to the parameters in Eqs. (4-11). By neglecting the oddereon, the terms where $i = 5$, 7, 9 and 10 will eliminate. Neglecting also the pomeron, terms with $i = 4$, 6 and 8 disappear and we get

$$B(s) = \frac{a(s) + b(s)L}{e(s)} \tag{24}$$

with terms where $i = 1$, 2 and 3. The expression for slope Eq. (1) with the single pomeron Eq.(8) with trajectory Eq. (9) reduces to:

$$B(s) = \frac{2\alpha_{1P}(a + bL + cL^2 + dL^3)}{e + fL + gL^2}, \tag{25}$$

where the parameters a, b, c, d, e, f are energy-independent. They may be easily expressed in terms of those Eq.(8):

$$
\begin{aligned}
a &= b_P e^{b_P \delta_P}[4b_P^2 e^{b_P \delta_P} + \pi^2 (e^{b_P \delta_P} - \epsilon_P)], \\
b &= \pi^2 (e^{b_P \delta_P} - \epsilon_P)^2 + 4b_P^2 e^{b_P \delta_P}(3e^{b_P \delta_P} - \epsilon_P), \\
c &= 12 b_P e^{b_P \delta_P}(e^{b_P \delta_P} - \epsilon_P), \\
d &= 4(e^{b_P \delta_P} - \epsilon_P)^2, \\
e &= 4b_P^2 e^{2b_P \delta_P} + \pi^2 (e^{b_P \delta_P} - \epsilon_P)^2, \\
f &= 8 b_P e^{b_P \delta_P}(e^{b_P \delta_P} - \epsilon_P), \\
g &= d = 4(e^{b_P \delta_P} - \epsilon_P)^2.
\end{aligned} \tag{26}
$$

In a similar way, the parameters a_i, b_i, c_i, d_i, e_i, f_i, g_i, and k_i in Eq. (23) may be related to those of Eqs. (4-11) (more complicated than in Eq. (26)).

Alternatively, the local slope $B(s,t)$ with unit pomeron intercept $\alpha(t=0)=1$ can be written as Ref. [37, 38]

$$B(s,t) = 2\alpha'(t)[b + F(s,t)L], \tag{27}$$

where

$$F(s,t) = 1 + \Phi'(\alpha)\Big[1 + \frac{\pi^2\Phi(\alpha)}{4L} + \Phi(\alpha)L\Big] \times\Big[[1+\Phi(\alpha)L]^2 + \frac{\pi^2}{4}\Phi^2(\alpha)\Big]^{-1}. \tag{28}$$

Equivalently, using Eq.(8) with the trajectory Eq. (9) we get for the slope Eq. (25).

Note that $F(s,t) \to 1$ as $s \to \infty$. Surprisingly, the function $F(s)$ decreases rapidly at small values of s, thus affecting the slope at small energies. It is close to 1 at high energies where the pomeron dominates.

References

References

[1] G. Antchev, et al., First measurement of elastic, inelastic and total cross-section at $\sqrt{s} = 13$ TeV by TOTEM and overview of cross-section data at LHC energies`arXiv:1712.06153`.

[2] G. Antchev, et al., Evidence for non-exponential elastic protonproton differential cross-section at low $|t|$ and $\sqrt{s}$=8 TeV by TOTEM, Nucl. Phys. B899 (2015) 527–546. `arXiv:1503.08111`, `doi:10.1016/j.nuclphysb.2015.08.010`.

[3] G. Antchev, et al., First determination of the parameter at s = 13 TeV probing the existence of a colourless three-gluon bound state, Submitted to: Phys. Rev.

[4] G. Antchev, et al., Measurement of proton-proton elastic scattering and total cross section at $\sqrt{s} = 7$ TeV, EPL 101 (2) (2013) 21002. doi:10.1209/0295-5075/101/21002.

[5] G. Barbiellini, et al., Small-angle proton-proton elastic scattering at very high energies (460 GeV^2 < s < 2900 GeV^2), Phys. Lett. B 39 (5) (1972) 663–667. doi:10.1016/0370-2693(72)90025-1.

[6] G. Cohen-Tannoudji, V. V. Ilyin, L. L. Jenkovszky, A model for the pomeron trajectory, Lett. Nuovo Cim. 5S2 (1972) 957–962, [Lett. Nuovo Cim.5,957(1972)]. doi:10.1007/BF02777999.

[7] A. A. Anselm, V. N. Gribov, Zero pion mass limit in interactions at very high-energies, Phys. Lett. 40B (1972) 487–490. doi:10.1016/0370-2693(72)90559-X.

[8] C.-I. Tan, D. M. Tow, Can Pions Be the Dominant Linkage in Multiperipheral Cluster Models?, Phys. Lett. 53B (1975) 452–456. doi:10.1016/0370-2693(75)90216-6.

[9] U. Sukhatme, C.-I. Tan, J. Tran Thanh Van, Elastic peak and hadron size from a t-channel viewpoint, Z. Phys. C1 (1979) 95. doi:10.1007/BF01450385.

[10] L. Jenkovszky, A. Lengyel, Low-$|t|$ structures in elastic scattering at the LHC, Acta Phys. Polon. B46 (4) (2015) 863–878. arXiv:1410.4106, doi:10.5506/APhysPolB.46.863.

[11] J. P. Burq, et al., Soft $\pi - p$ and pp Elastic Scattering in the Energy Range 30 GeV to 345 GeV, Nucl. Phys. B217 (1983) 285–335. doi:10.1016/0550-3213(83)90149-9.

[12] L. L. Jenkovszky, A. I. Lengyel, D. I. Lontkovskyi, The Pomeron and Odderon in elastic, inelastic and total cross sections at the LHC, Int. J. Mod. Phys. A26 (2011) 4755–4771. arXiv:1105.1202, doi:10.1142/S0217751X11054760.

[13] A. Ster, L. Jenkovszky, T. Csorgo, Extracting the Odderon from pp and $\bar{p}p$ scattering data, Phys. Rev. D91 (7) (2015) 074018. arXiv:1501.03860, doi:10.1103/PhysRevD.91.074018.

[14] A. N. Wall, L. L. Jenkovszky, B. V. Struminsky, Interaction of hadrons at high energies (in Russian), Sov. J. Nucl. Phys 19 (1988) 180–223.

[15] T. Csorgo, R. Pasechnik, A. Ster, Odderon and substructures of protons from a model-independent Levy imaging of elastic proton-proton and proton-antiproton collisionsarXiv:1807.02897.

[16] S. Wakaizumi, High Energy π-p Elastic Scattering and Constituent Multiple Scattering Model, Prog. Theor. Phys. 60 (1978) 1930–1932. doi:10.1143/PTP.60.1930.

[17] R. J. Glauber, J. Velasco, Multiple Diffraction Theory of $p\bar{p}$ Scattering at 546-GeV, Phys. Lett. 147B (1984) 380–384. doi:10.1016/0370-2693(84)90137-0.

[18] F. Nemes, T. Csorgo, M. Csanad, Excitation function of elastic pp scattering from a unitarily extended BialasBzdak model, Int. J. Mod. Phys. A30 (14) (2015) 1550076. arXiv:1505.01415, doi:10.1142/S0217751X15500761.

[19] G. Aad, et al., Measurement of the total cross section from elastic scattering in pp collisions at $\sqrt{s} = 7$ TeV with the ATLAS detector, Nucl. Phys. B889 (2014) 486–548. arXiv:1408.5778, doi:10.1016/j.nuclphysb.2014.10.019.

[20] M. Aaboud, et al., Measurement of the total cross section from elastic scattering in pp collisions at $\sqrt{s} = 8$ TeV with the ATLAS detector, Phys. Lett. B761 (2016) 158–178. arXiv:1607.06605, doi:10.1016/j.physletb.2016.08.020.

[21] R. J. N. Phillips, A dipole pomeron ansatz, Rutherford Lab. preprintt, PL-74-03 (1974).

[22] L. L. Jenkovszky, Phenomenology of Elastic Hadron Diffraction, Fortsch. Phys. 34 (1986) 791–816. doi:10.1002/prop.19860341202.

[23] J. Kontros, K. Kontros, A. Lengyel, Models of realistic Reggeons for t = 0 high-energy scattering, in: Elastic and diffractive scattering. Proceedings, 9th Blois Workshop, Pruhonice, Czech Republic, June 9-15, 2001, 2001, pp. 287–292. arXiv:hep-ph/0104133.

[24] J. Kontros, K. Kontros, A. Lengyel, Pomeron models and exchange degeneracy of the Regge trajectories, in: New trends in high-energy physics: Experiment, phenomenology, theory. Proceedings, International School-Conference, Crimea 2000, Yalta, Ukraine, May 27-June 4, 2000, 2000, pp. 140–144. arXiv:hep-ph/0006141.

[25] S. Donnachie, H. G. Dosch, O. Nachtmann, P. Landshoff, Pomeron physics and QCD, Camb. Monogr. Part. Phys. Nucl. Phys. Cosmol. 19 (2002) 1–347.

[26] http://durpdg.dur.ac.uk.

[27] G. Antchev, et al., Luminosity-independent measurements of total, elastic and inelastic cross-sections at $\sqrt{s}$ = 7 TeV, EPL 101 (2) (2013) 21004. doi:10.1209/0295-5075/101/21004.

[28] C. Patrignani, et al., Review of Particle Physics, Chin. Phys. C40 (10) (2016) 100001. doi:10.1088/1674-1137/40/10/100001.

[29] G. Antchev, et al., Luminosity-Independent Measurement of the Proton-Proton Total Cross Section at $\sqrt{s}$ = 8TeV, Phys. Rev. Lett. 111 (1) (2013) 012001. doi:10.1103/PhysRevLett.111.012001.

[30] G. Antchev, et al., Measurement of elastic pp scattering at $\sqrt{s}$ = 8 TeV in the Coulombnuclear interference region: determination of the ρ -parameter and the total cross-section, Eur. Phys. J. C76 (12) (2016) 661. arXiv:1610.00603, doi:10.1140/epjc/s10052-016-4399-8.

[31] P. Abreu, et al., Measurement of the proton-air cross-section at $\sqrt{s} = 57$ TeV with the Pierre Auger Observatory, Phys. Rev. Lett. 109 (2012) 062002. arXiv:1208.1520, doi:10.1103/PhysRevLett.109.062002.

[32] L. Jenkovszky, I. Szanyi, C.-I. Tan, Shape of Proton and the Pion Cloud, Eur. Phys. J. A54 (7) (2018) 116. arXiv:1710.10594, doi:10.1140/epja/i2018-12567-5.

[33] W. Broniowski, L. Jenkovszky, E. Ruiz Arriola, I. Szanyi, Hollowness in pp and $p\bar{p}$ scattering in a Regge modelarXiv:1806.04756.

[34] L. Jenkovszky, I. Szanyi, Fine structure of the diffraction cone: manifestation of t channel unitarity, Phys. Part. Nucl. Lett. 14 (5) (2017) 687–697. arXiv:1701.01269, doi:10.1134/S1547477117050065.

[35] L. Jenkovszky, I. Szanyi, Structures in the diffraction cone: The break and dip in high-energy protonproton scattering, Mod. Phys. Lett. A32 (22) (2017) 1750116. arXiv:1705.04880, doi:10.1142/S0217732317501164.

[36] A. O. Barut, D. E. Zwanziger, Complex angular momentum in relativistic s-matrix theory, Phys. Rev. 127 (1962) 974–977. doi:10.1103/PhysRev.127.974.

[37] L. L. Jenkovszky, B. V. Struminsky, The slope of the diffraction cone and the collider data (in russian), Sov. J. Nucl. Phys 39 (1984) 1252–1259.

[38] L. L. Jenkovszky, A. V. Kholodkov, D. M. Marina, A. N. Wall, Dipole pomeron and pp scattering, ITP preprint (1975).